ORIGINAL RESEARCH

How canopy shadow affects invasive plant species classification in high spatial resolution remote sensing

Javier Lopatin, Klara Dolos, Teja Kattenborn & Fabian E. Fassnacht

Institute of Geography and Geoecology, Karlsruhe Institute of Technology (KIT), Kaiserstraße 12, 76131 Karlsruhe, Germany

Abstract

Plant invasions can result in serious threats for biodiversity and ecosystem functioning. Reliable maps at very-high spatial resolution are needed to assess invasions dynamics. Field sampling approaches could be replaced by unmanned aerial vehicles (UAVs) to derive such maps. However, pixel-based species classification at high spatial resolution is highly affected by within-canopy variation caused by shadows. Here, we studied the effect of shadows on mapping the occurrence of invasive species using UAV-based data. MaxEnt one-class classifications were applied to map *Acacia dealbata*, *Ulex europaeus* and *Pinus radiata* in central-south Chile using combinations of UAV-based spectral (RGB and hyperspectral), 2D textural and 3D structural variables including and excluding shaded canopy pixels during model calibration. The model accuracies in terms of area under the curve (AUC), Cohen's Kappa, sensitivity (true positive rate) and specificity (true negative rate) were examined in sunlit and shaded canopies separately. Bootstrapping was used for validation and to assess statistical differences between models. Our results show that shadows significantly affect the accuracies obtained with all types of variables. The predictions in shaded areas were generally inaccurate, leading to misclassification rates between 65% and 100% even when shadows were included during model calibration. The exclusion of shaded areas from model calibrations increased the predictive accuracies (especially in terms of sensitivity), decreasing false positives. Spectral and 2D textural information showed generally higher performances and improvements when excluding shadows from the analysis. Shadows significantly affected the model results obtained with any of the variables used, hence the exclusion of shadows is recommended prior to model calibration. This relatively easy pre-processing step enhances models for classifying species occurrences using high-resolution spectral imagery and derived products. Finally, a shadow simulation showed differences in the ideal acquisition window for each species, which is important to plan revisit campaigns.

Introduction

Invasive plant species can alter ecosystem functioning and services, causing loss of biodiversity (Binggeli 1996) and water availability (Little et al. 2015), alterations in primary production and shifts in the N- and C-cycle (Vilà et al. 2011). Worldwide annual economic losses caused by biotic invasions are estimated to be one order of magnitude higher than those caused by all natural disasters together (Ricciardi et al. 2011). Mapping the arrival and spread of invasive species is hence crucial for risk assessments and to enable their control and eradication (Rocchini et al. 2015).

Remote sensing has been used to map invasive species occurrences in space and time, usually by combining field measurements with satellite or airborne data (e.g. see

review of Huang and Asner 2009). Recently, Unmanned Aerial Vehicles (UAVs) have been used to map the occurrence of invasive plant species. One advantage of UAVs is that they allow for flexible acquisitions of very-high-resolution imagery. This is important for early and accurate prediction of invasive species occurrences (e.g. Baena et al. 2017; Cao et al. 2018). Such UAV approaches are especially suitable to: (1) understand the invasion dynamics and processes at local scale through repetitive acquisitions, and (2) to derive reference data for large-scale satellite-based mapping of the invasions (Kattenborn et al. submitted).General benefits of UAV-based sensing include the possibility of optical data acquisition under cloudy conditions (e.g. de Sá et al. 2018) and the generation of orthomosaics that allows the comparison of temporal images comprising similar view angles (contrary to satellite-based high-resolution imageries were temporal data often differ in view angles; Anderson and Gaston 2013). Meanwhile, disadvantages of UAV-based sensing include their relatively small area cover and the relatively low radiometrical quality of the sensors (Hruska et al. 2012). UAV-based invasive species mapping has yielded high accuracies using different data types, like RGB or VNIR information (Michez et al. 2016; Alvarez-Taboada et al. 2017; Baena et al. 2017; Mafanya et al. 2017; Cao et al. 2018; de Sá et al. 2018), hyperspectral data (Cao et al. 2018) or 2D textural (Michez et al. 2016; Cao et al. 2018) and 3D structural (Kattenborn et al. 2014; Franklin et al. 2017) information derived from photogrammetric algorithms.

The development of user-friendly photogrammetric software with Structure-from-Motion (SfM) capabilities makes the processing of UAV data attractive for natural management practitioners with basic knowledge in geomatics. These SfM algorithms resolve the alignment of camera positions, which allows to generate orthorectified aerial imagery and 3D models without the allocation of ground control points (Westoby et al. 2012). Most studies that used such UAV products focused on mapping a single species using one or a few of the above-mentioned data types. However, a detailed comparison of data types for more than a single species is still missing. Such a study is relevant to assess the consistency of UAV-based invasive mapping requirements.

The extremely high spatial resolution and acquisition flexibility of UAV data offers new opportunities but also challenges. One drawback of very-high spatial resolution imagery is the increase of spectral within-class variability caused by canopy structure and shadows, which often hamper the separability of classes in pixel-based studies (Lopatin et al. 2017). Shadows result from the obstruction of light, causing a decrease of reflectance. In vegetation areas, cast shadows receive diffuse radiation (mostly Rayleigh scattering) from light scattered within the atmosphere or surrounding objects (Gu and Robles-Kelly 2014). In practice, shadows can lead to either a reduction or a total loss of the spectral signal of a canopy (Zhang et al. 2015), affecting the success of classification tasks (Saha et al. 2005; Liu and Yamazaki 2012). Therefore, careful consideration regarding acquisition time of the day is particularly important, as during some parts of the day shadows can cover a large part of the area of interest (Milas et al. 2017).

Many approaches have been developed to reduce the effects of shadows and improve classification performances. For instance, increasing pixel size has been found to be helpful to decrease within-class variability, usually improving classification performances when an ideal relation between pixel and crown size is obtained (Nagendra 2001). This ideal relation obviously depends upon the crown size and the canopy closure of the investigated species or ecosystems and can vary widely. Likewise, object-based analysis have been used to decrease the spectral variance at individual level (e.g. one spectral value per individual crown), obtaining in some cases higher classification performances than pixel-based approaches (e.g. Yu et al. 2006). However, obtaining a meaningful delineation of tree crowns is often challenging, especially for closed and overlapping canopies and in the presences of shadows (e.g. Nevalainen et al. 2017). Deep learning may also cope with shadows using the shadows as additional species-specific structure information. Nevertheless, deep neural networks usually need a large amount of training data which could hamper their use for practical applications with limited field data (Dyrmann et al. 2016). Other alternatives to address shadow effects are shadow correction methods, which consist in the radiometric enhancement of shaded pixels usually based on information extracted from neighboring non-shadowed regions (empirical methods; e.g. Singh et al. 2012) or on incident light sensor information (physical methods; e.g. Sismanidis et al. 2014). Yet, these methods may introduce noise and aberrations to the radiometrically corrected areas (e.g. Sismanidis et al. 2014) that could hamper class separability of spectrally similar classes, such as different plant species. This may be one reason why these methods have so far been mostly applied in urban contexts, where the class interfaces are often comparably clear.

In summary, averaging or smoothing the spectral information of adjacent pixels may improve classification performances, but at the risk of excluding meaningful variance of the target species' spectral signal due to canopy architecture. For these reasons, the use of only sunlit canopies for pixel-based species classification may be a suitable alternative to decrease within-class variability by excluding the undesirable information given by

shadows, while keeping important variations related to canopy architecture. While earlier UAV-based studies have reported negative influences of shadows in invasive species mapping (Franklin et al. 2017; Müllerová et al. 2017; de Sá et al. 2018), it is still uncertain whether or not the exclusion of shadows from the training data improves the UAV-based mapping results.

Hence, the main aim of this investigation was to assess the effects of shadows on the occurrence predictions of the woody species *Acacia dealbata*, *Ulex europaeus* and *Pinus radiata* using different combinations of spectral, 2D textural and 3D structural UAV-based data in central-south Chile. This aim is embedded in the overarching effort to develop a UAV-based work-flow to map individual target species with a minimum amount of training data and with possibly high accuracies for subsequent ecological analysis. We further investigated by means of simulations the role of the species-specific canopy structure in the production of daily shadows. This is important to assess ideal UAV acquisition periods and revisits.

Materials and Methods

The applied workflow consisted of six steps: (1) first, remote sensing data were acquired using unmanned aerial vehicles (UAV) in three different areas. Each area hosted one of the invasive species along with native woody species; (2) then, canopies of the invasive species were manually delineated by visual interpretation of the UAV data to create training and validation data; (3) shadows occurring inside the canopies were identified using an automatic approach; (4) independent variables were created from the UAV data, to create the datasets needed for modeling (MaxEnt); (5) MaxEnt models were trained to estimate relative likelihoods of occurrences of each invasive species. Results in sunlit and shaded canopy areas were compared to assess the relative effects of shadows in the classification performances; (6) finally, simulations were carried out to assess the effect of day-time and species-specific canopy shape on the quantity of shadows occurring in the corresponding canopies.

### Study sites and target species

Central-south Chile is considered a world's biodiversity hot-spots (Myers et al. 2000), harboring a high level of endemism because of its geographical isolation. Furthermore, in central-south Chile, species from the sclerophyll forest ecosystems of the North and the deciduous *Nothofagus* forests in the souths are co-occurring which leads to a particularly high biodiversity. This biodiversity is threatened by diverse biotic and abiotic factors, including pronounced land-use changes occurring over the last decades but also invasive species which are global drivers of extinctions; they compete with native species for resources, and can alter the community dynamics (Binggeli 1996).With the arrival of the colonists, areas formerly cover by native forests and/or shrublands were cleared for agriculture and silviculture purposes, causing the introduction of several European and Oceanic invasive plants (Holmgren et al. 2000). We studied the presence of three woody invasive species, *Pinus radiata*, *Ulex europaeus* and *Acacia dealbata*, in three study areas including the 'Maule', the 'Biobio' and the 'Los Lagos' regions (Fig. 1). *P. radiata* was introduced in the Maule region for timber production (Clapp 1995), whereas *U. europaeus* was introduced as a hedge plant to contain livestock (Norambuena et al. 2000) Finally, *A. dealbata* was introduced for ornamental purposes (Fuentes-Ramírez et al. 2011). These species have been found to be very noxious worldwide, but particularly in South American countries (Chile, Argentina and Brazil; Richardson et al. 2014), causing serious losses in biodiversity and affecting water supply (e.g. Little et al. 2015). Here, the three invasive species dominantly occurred in different parts of central-south Chile. We decided to use more than a single target species to develop an understanding of the reliability and stability of the proposed methods (Fig. 1). All of the targeted species are suspected to endanger both native flora and fauna.

UAV data acquisition and derivation of presence data for the target species

We performed one UAV flight for each study site using an octocopter (Okto-XL, HiSystems GmbH, Germany). Flights were carried out in March, November and December 2016 for *P. radiata*, *U. europaeus* and *A. dealbata*, respectively, partly overlapping the flowering season for *A. dealbata* and *U. europaeus*. The octocopter was equipped with two optical sensors: an RGB standard consumer-grade camera (Canon 100D, 28 mm focal length, 5196×3464 pixels) and a snapshot hyperspectral camera (OXI-II, Gamaya, Switzerland) with 41 spectral bands ranging from 450 to 950 nm and a 10 nm bandwidth. The flight plans aimed for an average of 90% of forward and 70% of sideward overlap for both sensors at 150 m above ground.

Photogrammetric point clouds, digital surface models (DSM) and orthomosaics were obtained for both sensors using a standard Structure-from-Motion (SfM) pipeline (Agisoft Photoscan, Agisoft, Russia; Kattenborn et al. 2018a). The point cloud densities was at average ~1000 points/m^2, whereas the selected pixel size for the final digital surface models (DSM) and RGB and hyperspectral orthomosaics were ~0.1 m. The point cloud was filtered using TreesVis (Weinacker et al. 2004) to ensure uniform spaces between points of ~0.03 m. The corresponding Agisoft photoscan parameters can be found in Table S1. The UAV GPS trajectory logged during the flights were used to automatically georeference the tiles during the SfM workflow. Finally,
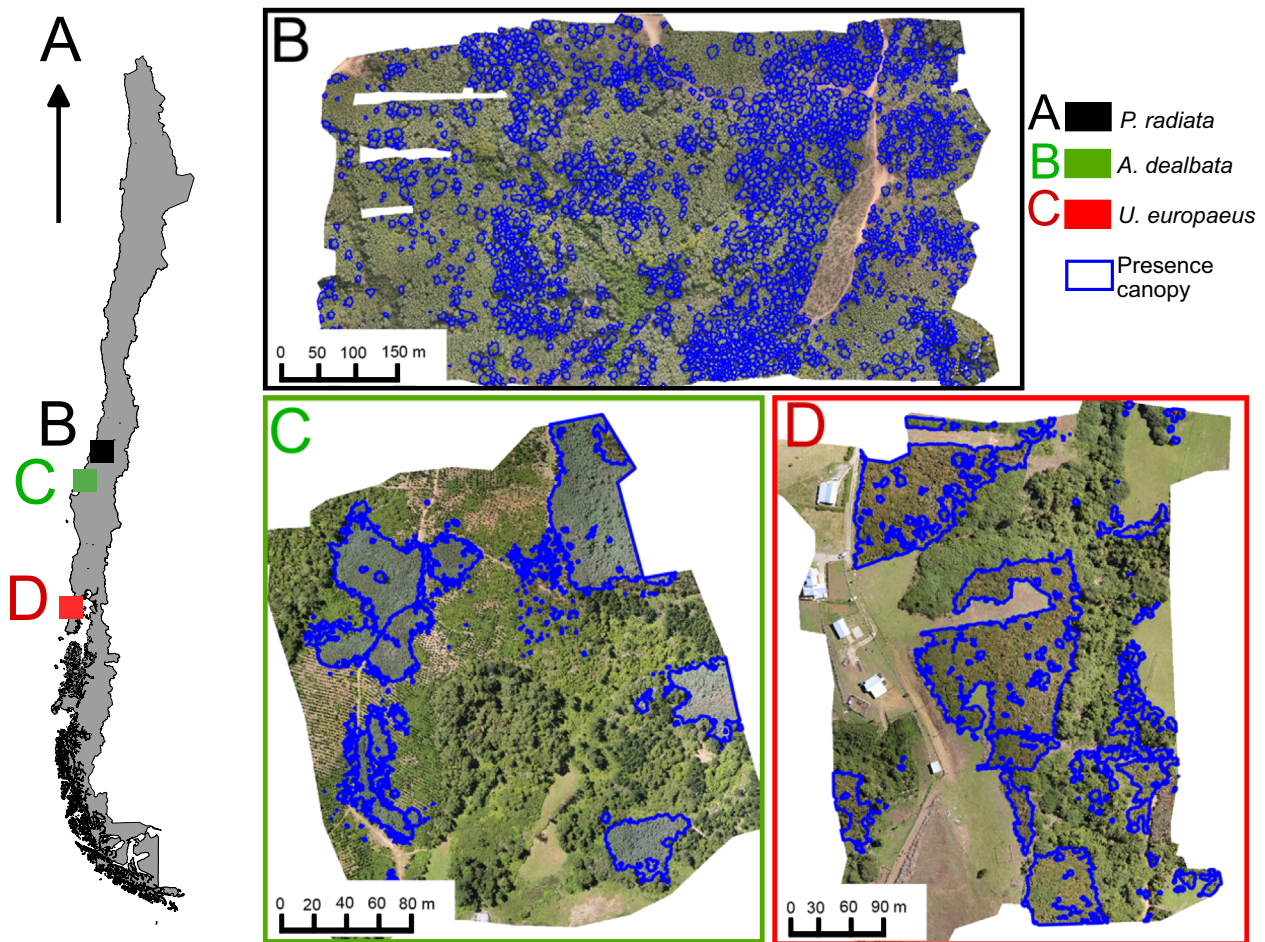
Figure 1. (A) Study areas in central-south Chile. (B–D) show the UAV-based RGB imageries. Blue polygons indicate the presence of the invasive species.

hyperspectral reflectance data were obtained by calibrating the raw data with a reference panel with known reflectance, placed in the field during the flights. The final coverage of the acquired scenes were ~7, 18 and 37 hectares for *U. europaeus, A. dealbata* and *P. radiata,* respectively.

Costs for assessing the invasion status of a species via field sampling are usually high and may lead to biased results (Cacho et al. 2006; Kaplan et al. 2014). Instead of field sampling, we hence used the UAV orthomosaics to manually delineate all occurring canopies of the target invasive species (presences) in each flight (Fig. 1). The canopy characteristics of the examined target species differed clearly in terms of their structural and spectral (e.g. flowering) properties to the native vegetation which enabled reliable delineations.

Shadow detection

All shadows occurring inside the manually delineated invasive species canopies (UAV data acquisition and derivation of presence data for the target species) were

determined using an RGB-based histogram thresholding, which gives relative high accuracies while being straight-forward to implement (Adeline et al. 2013). The thresholds were derived by visual interpretation (e.g. Adeline et al. 2013); where values below 80 digital number (DN; from a range of 0–255 DN; ~30% reflectance) of the red band showed a reliable separation between sunlit and shaded canopies for the three species. Shaded areas accounted for ~20% of the invasive species canopies in all cases. Sunlit canopies were obtained by excluding the shaded areas from the delineated target species canopies.

Derivation of independent variables from the UAV data

Two types of spatial textural metrics were obtained from the RGB products: (1) a set of 2D texture layers based on the gray-level covariance matrix (GLCM; mean, variance, homogeneity and entropy), and (2) a set of 3D structure layers derived from a multi-scale analysis of the

photogrammetric point cloud (Brodu and Lague 2012). Each metric type was calculated in 10 different spatial scales ranging from 0.25 to 4 m window size (using a 0.25 and 0.5 m step between 0.25–1 m and 1–4 m, respectively). The different scales were chosen to derive information from both branch- and canopy-level. The GLCM indices were obtained by applying a moving window approach where each pixel was assigned with the above-mentioned metrics of the neighboring pixels using the original RGB images at a spatial resolution of 0.1 m. The 3D structure algorithm processed principal component attributes at different spatial scales (3D neighborhood) for each point in the photogrammetric point cloud, representing the local dimensionality characteristics (shape and density) of the canopy (CANUPO algorithm; Brodu and Lague 2012). Metrics calculated from the point clouds were rasterized (0.1 m pixel size) to facilitate the analysis. The R-package 'glcm' was used to create the GLCM, whereas the CANUPO toolbox along with LAStools and Python 3.6 were used to create the 3D structure raster components.

In total, we created eleven datasets by combining layers of spectral (i.e. RGB and hyperspectral), 2D textural and 3D structural information (Table 1). RGB and hyperspectral data were not combined as they contain redundant information.

Modeling and validation

We used the maximum-entropy (MaxEnt) classifier (Phillips et al. 2006) to model the occurrence of the invasive species for each UAV dataset. MaxEnt is a one-class classifier that uses presence (labeled) and background (unlabeled) data to create a relative likelihood distribution (between 0 and 1) of the invasive species. MaxEnt has shown reliable results with remote sensing data (Mack et al. 2016; Skowronek et al. 2017; Stenzel et al. 2017). From an operational point of view, the application of MaxEnt is very promising, as the delineation of training data of unwanted classes (e.g. other tree species, bare ground and water bodies) are not required during modeling, which notably decreases pre-processing or sampling efforts. In each study area, 500 presence samples were selected by randomly sampling pixels inside the delineated polygons of the invasive species crowns, whereas 2,000 backgrounds pixels were randomly sampled from the whole area. We used the R-package 'dismo' with default setting for the MaxEnt modeling.

To test how the 11 UAV-based independent variables (Table 1) were influenced by the presence of shadows, two types of models were tested: (1) MaxEnt models calibrated using all available presence data, including pixels of sunlit and shaded canopies, and (2) MaxEnt models calibrated using only presence data of sunlit canopies.

A variable selection was applied to each model. Variable selection minimizes the chances of overfitting (Merow et al. 2013) and enhances model transferability (Duque-Lazo et al. 2016). First, MaxEnt classifications using all available variables were performed using a 10-fold cross-validation. Then, the variables that obtained a permutation importance <5% were dropped. Finally, from the remaining variables only the variables with shared correlations $r < 0.8$ were kept, whereas in case of correlation $r > 0.8$ the variable with higher permutation importance was considered. The particular method applied here was selected due to its lower CPU processing time compared to iterative methods (e.g. Jueterbock et al. 2016).

An iterative validation based on stratified bootstrapping (Kohavi 1995) was used to obtain the distribution of model accuracies and rel. likelihood predictions that enable the estimation of significant differences among independent variables. The model performances were evaluated for sunlit and shaded canopies separately. We used a stratified bootstrapping procedure with 100 repetitions. In each repetition, we randomly selected samples with replacement for the presence and background datasets, whereas we used the samples that were not selected in both cases (~36%) as holdout samples for validation. We evaluated the model performances in terms of area under the curve (AUC), Cohen's Kappa, sensitivity (true positive rate) and specificity (false positive rate). We selected the thresholds for Kappa, sensitivity and specificity according to the values of maximum Kappa and (sensitivity + specificity), respectively.

Table 1. Datasets for each invasive species.

# Model	Datasets included (number of variables)	Model abbreviation
1	RGB (3)	rgb
2	Hyperspectral (41)	hyper
3	Texture (40)	text
4	Structure (10)	struct
5	Structure + Texture (50)	structtext
6	Structure + RGB (13)	structrgb
7	Structure + Hyperspectral (51)	structhyper
8	Texture + RGB (43)	textrgb
9	Texture + Hyperspectral (81)	texthyper
10	Structure + Texture + RGB (53)	structtextrgb
11	Structure + Texture + Hyperspectral (91)	structtexthyper

Texture corresponds to the GLCM variables, whereas Structure corresponds to the CANUPO 3D variables. All datasets were tested at ~0.1 m pixel size.

We used a one-sided bootstrap pair test to check for significant differences ($\alpha = 0.05$) in the obtained accuracy (AUC, Kappa, sensitivity and specificity) between models. We specifically tested if: (1) models performed significantly better in sunlit canopies than in shaded canopies; (2) models excluding shaded canopies in calibration performed significantly better in sunlit areas than models including shadows in calibration; (3) models including shadows in calibration performed significantly better in shaded areas than models excluding shadows in calibration; (4) models including spectral, 2D textural and 3D structural information performed significantly better than one variable type alone. This bootstrap test has been applied in earlier studies following similar approaches (Lopatin et al. 2016, 2017; Castillo-Riffart et al. 2017; Araya-López et al. 2018).

Species occurrence maps

Relative likelihood prediction maps of the invasive species occurrences were obtained by estimating the median value of the 100 bootstrap iterations per pixel. We further estimated the coefficient of variation (CV) of each pixel as a measure of model stability during bootstrapping, where pixels with low CV denote higher predictive stability. Finally, binary maps of the invasive species presence were produced using the median predicted likelihood maps and applying the median threshold value according to Kappa.

Shadow fraction simulation analysis

Species-specific canopy architecture influences the way species interact with light and hence their reflectance (e.g. Kattenborn et al. 2018b). The fraction of shadows is highly dependent on the sun-angle during the acquisition of optical remote sensing data. Understanding the dynamics of shadow fractions in the acquired images as a function of the sun-angle is hence important to assess the potential effects on classification accuracies and to plan optimal data acquisition windows accordingly. This is particularly interesting for UAV applications which allow for a comparably flexible selection of the acquisition times.

To model how the three-dimensional canopy architecture of the three examined species influence the production of shadow fractions throughout the course of a day, we simulated the shadows using the ~0.1 m DSMs of the study areas. Here, we varied the solar elevation and azimuth of beginning, middle and end of the 2017–2018 summer season along a daily period between 09:00 and 18:00 h. We masked out all the canopies that did not correspond to the studied invasive species to exclude the effects of the neighboring canopies. We used the R-packages 'insol' and 'suncalc' for the analysis.

Results

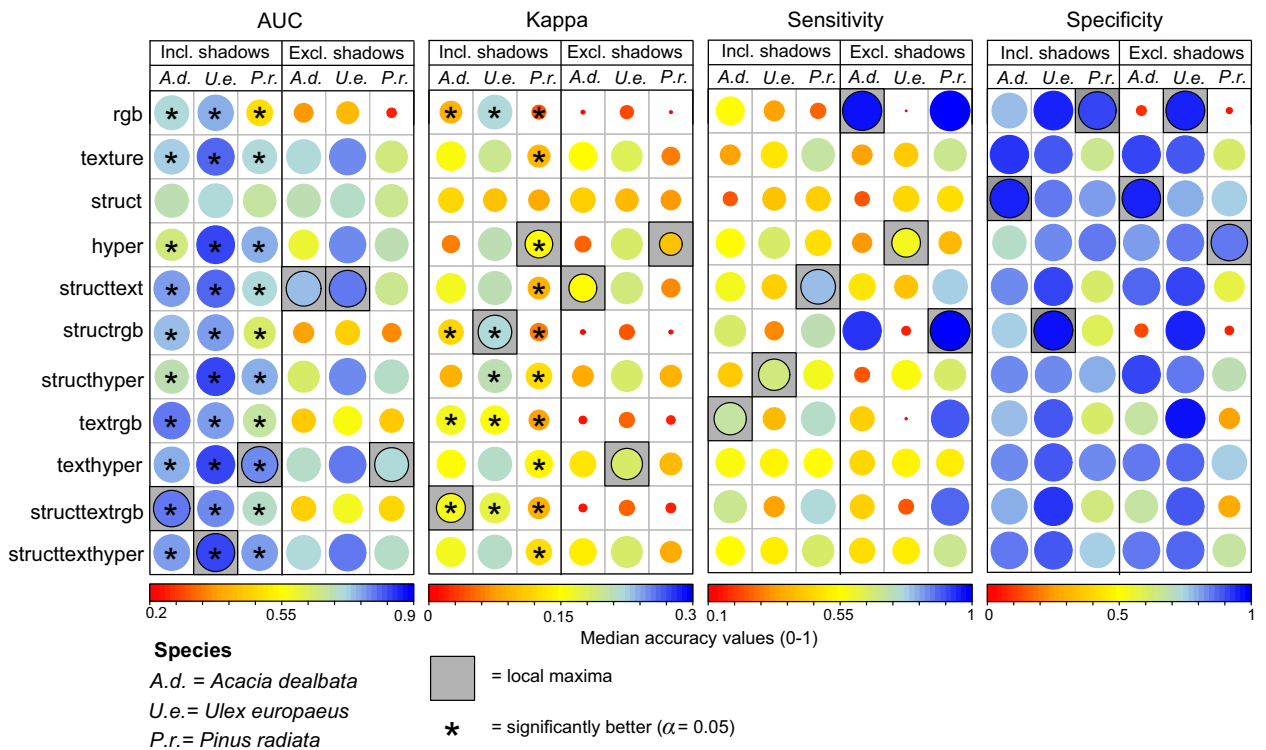### Model performances and independent variable selection

The accuracies of the models based on all presence samples (sunlit + shadows) and only sunlit canopies are summarized in Figure 2, whereas Table 2 shows the occasions where each model performed significantly better in sunlit areas than in shaded areas. Overall, model accuracies in terms of Kappa were significantly higher in sunlit canopies compared to shaded areas in almost all cases. Moreover, the accuracies in sunlit canopies improved when excluding shaded samples from the calibration data. Inaccurate classifications were found in shaded canopies even when shadows were included in calibration; presenting median Kappa values <0.3, uneven performances of sensitivity and specificity, and coefficient of variation (CV) values near 100% for Kappa and specificity (Fig. S1). Concurrently, AUC values remained high in the shadow areas, showing less sensitivity to the effects caused by shadows than Kappa. Classification accuracies were higher for *A. dealbata* than for *P. radiata* and *U. europaeus.*

Models including RGB information improved significantly ($\alpha = 0.05$) when excluding shadows from the calibration data, whereas hyperspectral, 2D textural and 3D structural data alone did not vary significantly among model types (Fig. 2). Sensitivity and specificity were found to vary more than AUC and Kappa, presenting few stable significant differences among model types. When using one type of independent variable, spectral information outperformed 2D textural and 3D structural information in most cases in terms of Kappa: RGB was found to be the best single option for *A. dealbata*, whereas hyperspectral information was the best variable for *U. europaeus* and *P. radiata*. The worst type of independent variable for *A. dealbata* and *U. europaeus* was the structural information, whereas for *P. radiata* it was RGB. When combining multiple types of independent variables, the best data combination for *A. dealbata* and *P. radiata* was RGB + texture + structure. For *U. europaeus* the best combination of independent variables was hyperspectral + texture + structure. Only for *U. europaeus* the use of a single variable type (i.e. hyperspectral) resulted in higher performances compared to the combination of independent variable types. Significant differences between the use of the best single independent variables and the best combination of variables were obtained for *U. europaeus* and *P. radiata* in terms of Kappa. Only *A. dealbata* and *U. europaeus* showed significant differences

A   Performances obtained for sunlit canopies
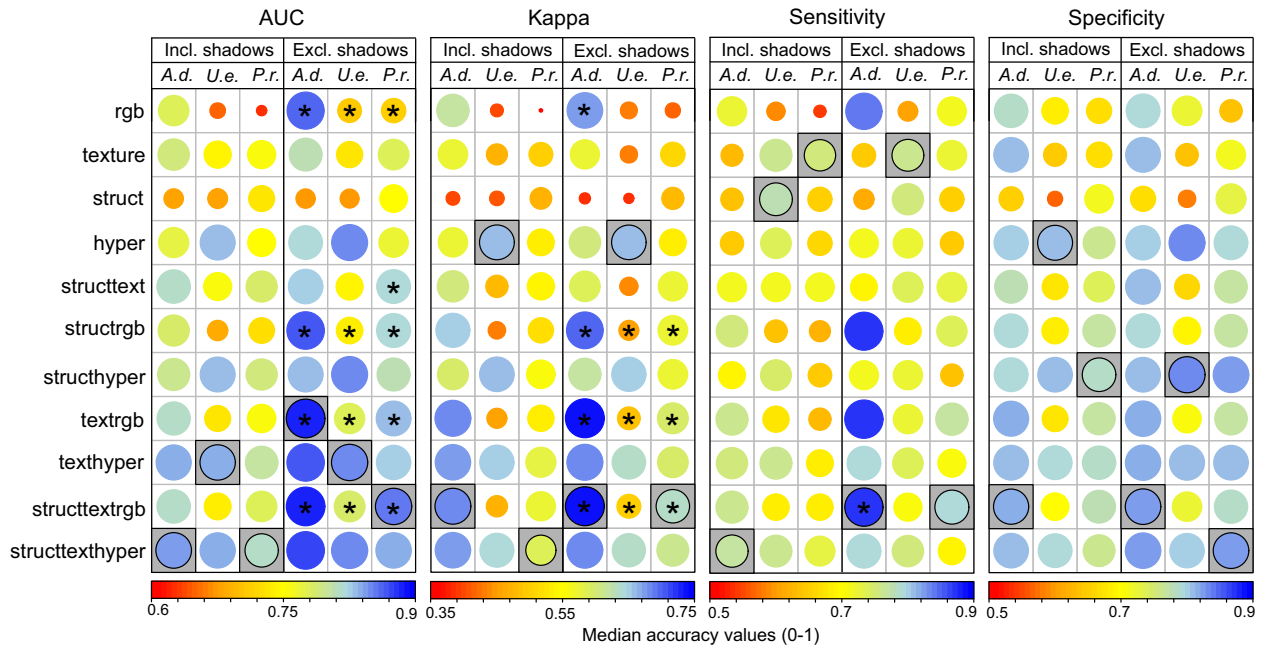
B   Performances obtained for shaded canopies

Species

A.d. = Acacia dealbata
U.e. = Ulex europaeus
P.r. = Pinus radiata

= local maxima

* = significantly better (α = 0.05)

Figure 2. Model performances for sunlit (A) and shaded (B) canopies using models that include (incl.) and exclude (excl.) shadows in the calibration data. The median iterative values are presented, with dot size scaled to the values. A.d. = *Acacia dealbata*; U.e. = *Ulex europaeus*; P.r. = *Pinus radiata*. * depicts significant (α = 0.05) improvements of the models: (A) shows significant improvements of models excluding shaded canopies. Contrary, (B) shows significant improvements of models including shaded canopies.

Table 2. Significant differences in terms of model performance between evaluations in sunlit and shaded canopies.

	AUC						Kappa						Sensitivity						Specificity					
	Incl. Shadows			Excl. Shadows			Incl. Shadows			Excl. Shadows			Incl. Shadows			Excl. Shadows			Incl. Shadows			Excl. Shadows		
	A.d.	U.e.	P.r.	A.d.	U.e.	P.r.	A.d.	U.e.	P.r.	A.d.	U.e.	P.r.	A.d.	U.e.	P.r.	A.d.	U.e.	P.r.	A.d.	U.e.	P.r.	A.d.	U.e.	P.r.
rgb	***	**	**	***	***	***	***		**	***	***	***		*		**	**			**			*	*
texture	**	***	**	***	**	***	***	**	***	***	*	***	**	**		**			*	***		*	**	*
struct	***		**	***		**	*		***	*		**	*			**						**		
hyper	***			***			***	***	***	***	***	***				*								
structtext	***	***	***	***	***	***	***		***	***	***	***			**		*			***	*		***	*
structrgb	***	*	**	***	***	***	***	***	***	***	***	***	*							**				
structhyper	***		**	***	**	***	***	**	***	***	***	***				*								
textrgb	***		*	***	***	***	***	***	***	***	***	***	**	*		**				*	*			
texthyper	***		***	***	***	***	***	**	***	***	***	***	*				*							
structtextrgb	***		***	***	***	***	***	***	***	***	***	***	**	*		**				**	**		**	*
structtexthyper	***		***	***	***	***	***	***	***	***	***	***	**			**							*	*

Significance levels (α): ***0.001, **0.05, *0.1.
Model including (incl.) and excluding (excl.) shadows during calibration. Marks depict for which variable combinations and calibration data the performance was significantly better for sunlit than in shaded areas. A.d. = *Acacia dealbata*; U.e. = *Ulex europaeus*; P.r. = *Pinus radiata*.

among variable types in terms of sensitivity and specificity, respectively (Fig. S2).

When combining hyperspectral, 2D textural and 3D structural information the variable importance (assessed by permutations of MaxEnt) was higher for spectral and 2D textural information than for 3D structural information (Fig. 3). Nonetheless, for *P. radiata* the importance of 3D structural information was higher than for the other species. In most cases, 2D textural information obtained at canopy-level (1–4 m window size) were more important than information obtained at branch-level (0.25–1 m window size), except for *U. europaeus* which also selected branch-level variables. In all cases 3D structural information was only relevant at canopy scales.
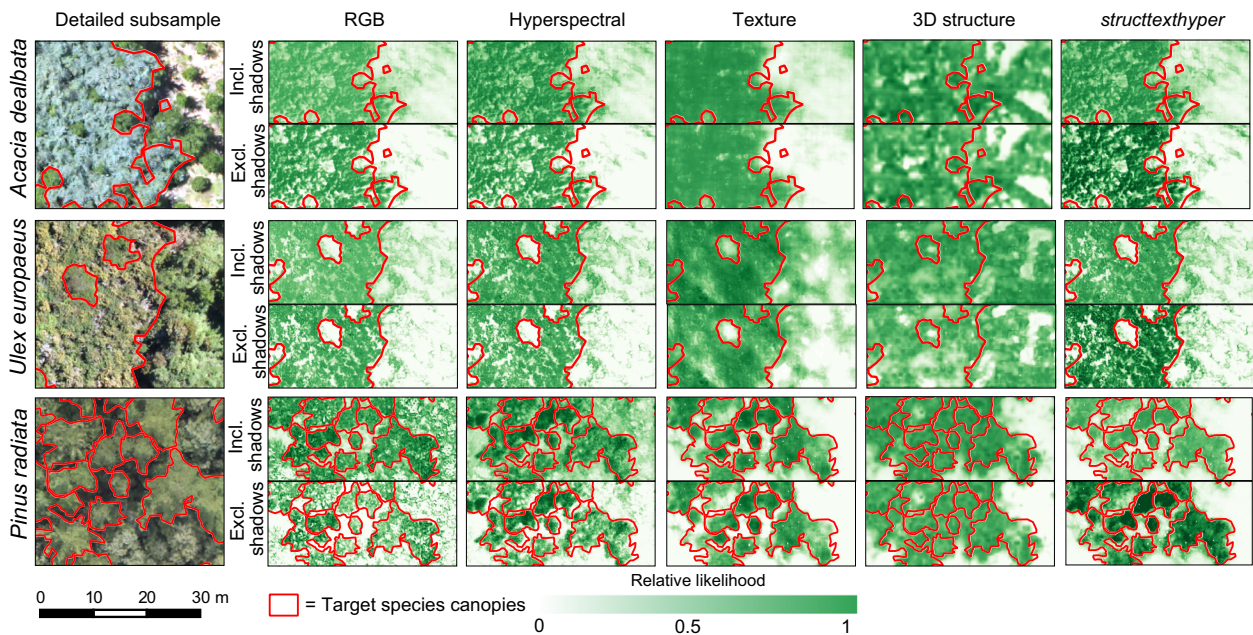
Model predictions

The predicted rel. likelihood values using different independent variables (Fig. 4) indicate good performances of the spectral information for identifying *A. dealbata* and *U. europaeus*. Predicted patterns improved for *P. radiata* when combining spectral, 2D textural and 3D structural information. All models had a general tendency toward overpredictions.

In Figure 5, examples of the predicted rel. likelihood based on the best models according to Kappa are displayed. Models where shadows were excluded during calibration obtained higher contrasts between the target species (higher median and lowed CV rel. likelihood values) and the rest of the scene (lower median and higher CV rel. likelihood values). However, models calibrated using only sunlit canopies resulted in occurrence maps with a higher amount of canopy gaps (pixels with low rel. likelihood), corresponding to areas with shadows. Hence, models excluding shadows from the calibration data also yielded high false negative rates (lower specificity). The exceptions were models based on 2D textural information, which due to their multi-level window sizes were able to fill the canopy gaps (Fig. 4).

The relative likelihood, obtained in the shadowed areas by models including shaded canopies in the calibration data, was predominately lower than the Kappa threshold. Hence, binary presence/absence maps also presented large amounts of false negatives. The amount of false negatives (i.e. presences falsely predicted as absence) inside the invasive species crowns ranged between ~20% and ~13%, which corresponded to ~100% and ~65% of the shadow areas for the models excluding and including shadow during calibration, respectively. Likewise, false positives outside the target crowns decreased by ~17% when excluding shadows during calibration (e.g. Fig. 5 blue circles). This can be seen in the increase of sensibility of almost all models when excluding shadows from the calibration data (Fig. 2a). Finally, the total amount of area covered by the
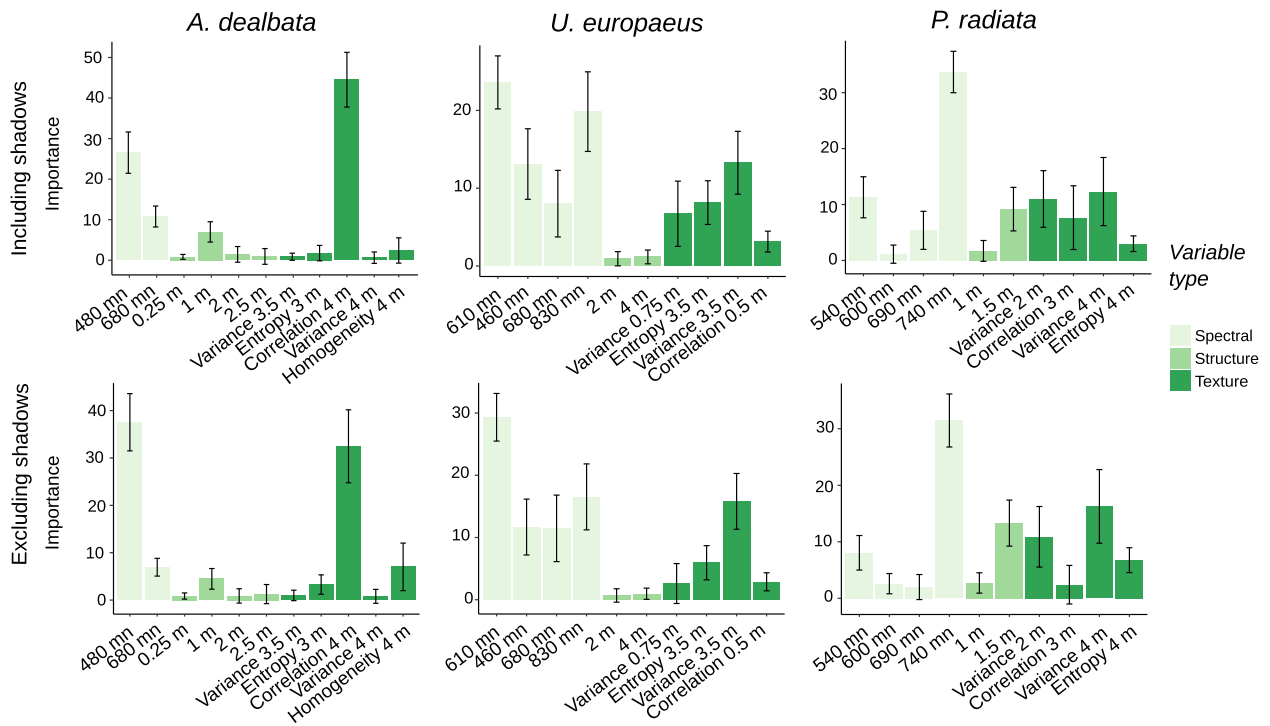
Figure 3. Variable importance based on MaxEnt permutation for the models including and excluding shaded canopies in the calibration data. Median and standard deviation values of the iterative validation are represented by barplots and error bars, respectively.

Figure 4. Relative likelihood predictions using different independent variables. Models including and excluding shadows during calibration are presented.
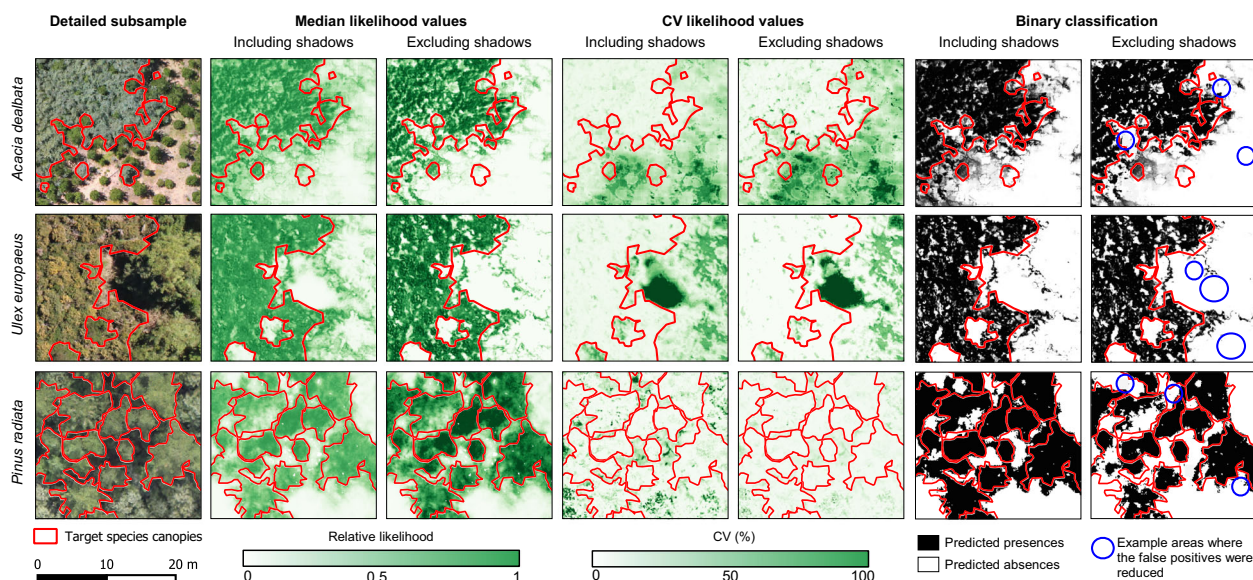
Figure 5. Comparison of species occurrence maps between models including and excluding shaded canopies in the calibration data. Models presented: *A. dealbata* and *P. radiata* = strcttextrgb, *U. europaeus* = hyper.

invasive species canopies according to the binary maps of the models excluding shadows were ~27%, 29% and 30% for *A. dealbata*, *U. europaeus* and *P. radiata,* respectively. Models including shadows during calibration tended to overestimate the invasive species presence's with ~5% in all three species.

Shadow fraction simulation analysis

The simulations using the digital surface models (DSM; Fig. 6) showed that the optimal acquisition window (here defined as less than 20% shadows) varied among the considered species: *U. europaeus* and *P. radiata* obtained the longest and the shortest optimal acquisition period, respectively. The simulated proportion of shaded crowns during the course of the day (Fig. 6c) confirms that *P. radiata*'s canopies are shaded during a large portion of the day, whereas *U. europaeus* canopies are mostly sunlit.

Discussion

Shadows effects in MaxEnt models

Our analyses show that MaxEnt predicted likelihood values for shaded areas are inaccurate even when including shaded canopies during calibration (Fig. 2b). This leads to a general decrease contrast in rel. likelihood between the actual target species canopies and the rest of the landscape which increases the false positive rate (Fig. 5). Generally, between 65% and 100% of shaded parts of the target species were wrongly classified as absences. This ~13–20% wrongly

classified canopy area could hamper the use of the predicted occurrences for subsequent ecological analyses, such as the analysis of detailed invasion dynamics or to upscale the mapping of the invasive species to larger scales via satellite imagery (e.g. Kattenborn et al. submitted). These errors were comparable to other UAV-based invasive species mapping studies which obtained user accuracies between 60% and 95% (Alvarez-Taboada et al. 2017; Mafanya et al. 2017; Müllerová et al. 2017; Cao et al. 2018).

Few UAV-based studies discussed the effects caused by shadows on their classification results: de Sá et al. (2018) found that shadows significantly decreased model accuracies in the detection of species of the genus *Acacia* under sunny conditions, whereas acquisitions under diffuse light conditions caused by clouds significantly increased classification accuracies due to a reduction cast shadows. Nevertheless, cloudy conditions would also decrease the separability of spectrally similar classes (Zhang et al. 2015). In contrast, other studies showed that the inclusion of shadows into the training samples improved classification performances (Milas et al. 2017; Ishida et al. 2018). However, these classifications involved the separation of classes with less overlapping spectral signatures compared to the classes considered here. When the separation of a species from other species with similar spectral characteristics is pursued, the high amount of intraspecific variance can hamper pixel-based classification performances (Lopatin et al. 2017).

According to Milas et al. (2017), the amount of detected shadows vary depending on the spatial resolution, which we did not consider in this investigation. We also did not account for gradients of shadows in our
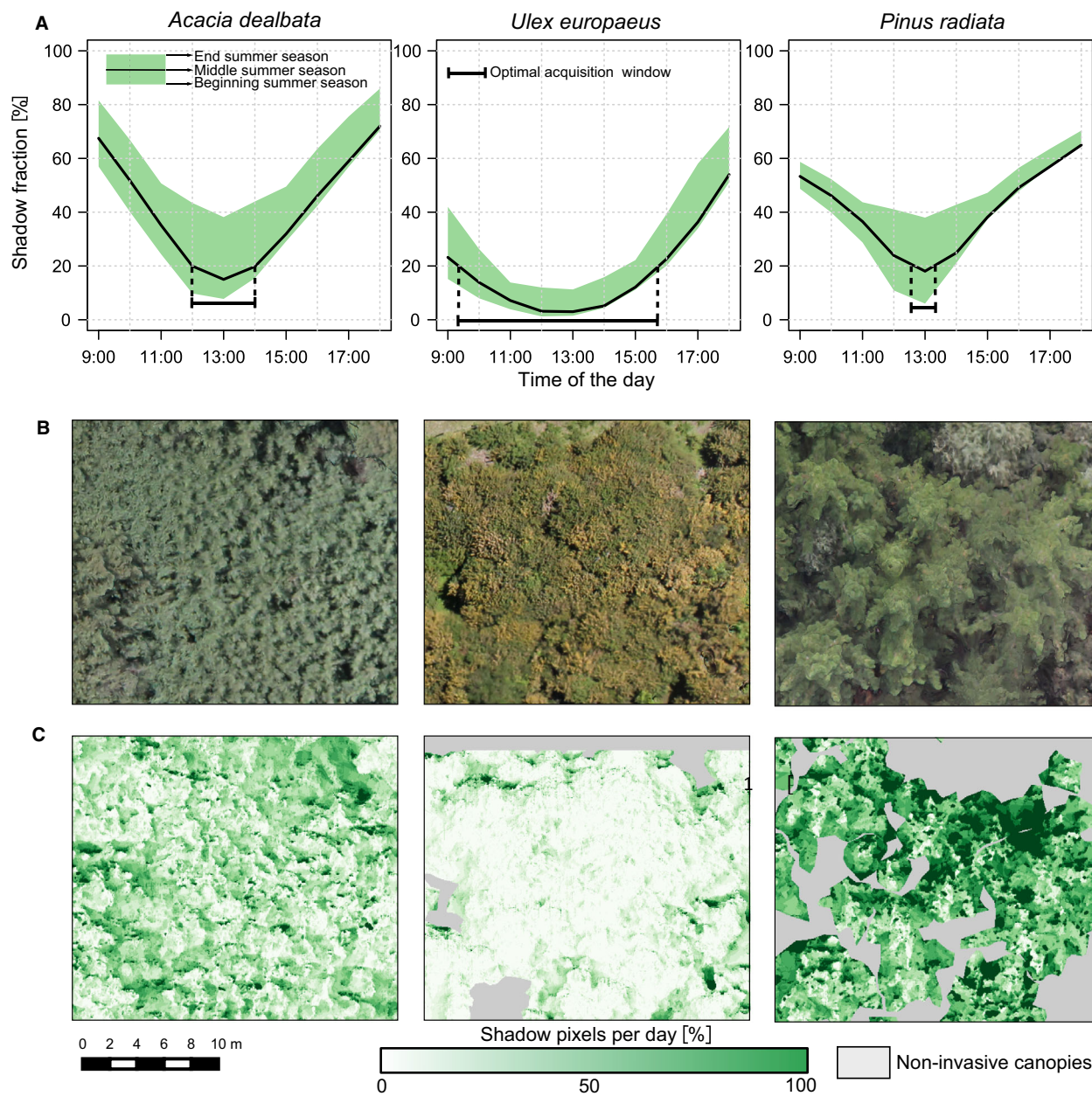
Figure 6. Shadow simulation using the digital surface models (DSM) and the sun elevation and zenith angles corresponding to beginning, middle and end of the summer season (i.e. 21 December 2017, 04 February 2018 and 20 March 2018 of each study site: (A) shows the simulated shadow fractions between 9:00 and 18:00 h; (B) shows an RGB subsample of the target species canopies; and (C) shows the number of times (in percentage) that the pixels of the target canopies were under shadow for the daily period of the middle summer day (04 February 2018).

analyses (e.g. Milas et al. 2017), but used a binary classification. Nevertheless, from our results (i.e. between 65% and 100% of misclassification rate inside shaded areas) we assume that shadows in general negatively affect the performance of pixel-based classification algorithms and that should be avoided whenever possible. However, we do not dismiss the possibility that shadows could at some point enhance classifications when algorithms that

efficiently exploit complex neighborhood information are used (e.g. convolutional neural networks). This assumption could be supported by the fact that all three species showed differences in their daily shadow fractions and temporal distributions (Fig. 6).

The amount of cast shadows could be reduced (and hence the false negative rate) by acquiring the UAV data at an ideal time. In our simulation exercise, this ideal

time was consistently identified to be around ~13:00 h local time. The shadow simulation performed in our study sites showed that the width of the optimal temporal acquisition window varied greatly according to the species-specific canopy characteristics (Fig. 6). At the spatial scales considered in this study, *U. europaeus* usually builds more homogeneous canopies, yielding generally less shadow fractions in comparison to *P. radiata*, which depicted the highest amount of shaded areas during the day (Fig. 6c). These differences are explained by the canopy architecture of the species, as the spherical crown shapes from *U. europaeus* and *A. dealbata* results in relatively homogeneous canopy structures when canopies are closed. This leads to generally low shadow fractions. Contrary, the vertical conical shapes and the star-shape branching pattern of *P. radiata* lead to high shadow fractions. Even in high density stands there are relative distinct height differences between the higher and the lower parts of the neighboring crowns. Because we were mostly interested in the species-specific shape characteristics of the invasive species canopies, we did not include the canopies of the native species in the analysis. In highly heterogeneous interspecific stands such as the one presented in the *P. radiata* flight, neighboring species with different canopy shapes and sizes may also influence the shadow fraction of the general canopy.

In order to minimize shadows and their effects on classification tasks in UAV-based species mapping applications, species-specific considerations regarding data acquisition are recommended. The approach proposed here to simulate shadows using digital surface models can be a useful tool to assess the shadow fractions during the course of a day and to plan revisit acquisitions accordingly.

The canopy structure of the invasive species also differs from the structure of the native forests and shrublands. Chilean native forests of the area tend to growth in highly heterogeneous stands of broadleaf species (e.g. tree species richness between 4 and 30 species in 225 m^2 plots; Lopatin et al. 2016) with many understorey species. On the contrary, woody individuals in shrublands tend to growth in a scatter manner (Luebert and Pliscoff 2006). Both vegetation types contrast with the clustered growth and relatively uniform canopies of *A. dealbata* and *U. europaeus* (e.g. Fuentes-Ramírez et al. 2011) and the conical canopy shape of *P. radiata*. These characteristics make the selected invasive species suitable for experimentation with remotely sensed data, as they clearly differ from the native stands in terms of structure and growth strategy and hence should be comparably easy to detect.

Variable importance

We found that AUC responses were not sensible to the observed negative effects of shadows in the model predictions, hence we will refer only to Kappa for general tendencies. Our results show that the best combination of independent variables depends on the target species, and that shadows significantly affected models using all types of independent variables. Models including RGB depicted largest improvements when excluding shadows from calibration, whereas 3D structure varied the least (Figs. 2a and 5). The models combining RGB, 2D textural and 3D structural information yielded high performances for *A. dealbata* and *P. radiata*, maybe due to the eye-catching silver and dark color of the species leaves, respectively (see detailed subsample of Fig. 4). This could be advantageous from an operational point of view as the cost and processing efforts of RGB data are generally lower than for hyperspectral data. This corroborates the findings of de Sá et al. (2018), which also classified a species of the genus *Acacia* (i.e. *A. longifolia*) with high accuracies using RGB imagery.

Contrary, *U. europaeus* was mapped with highest accuracies when applying hyperspectral data alone, which could be due to its rather homogeneous canopy with few structural and hence textural differences (Fig. 6c). On the other hand, the 3D structure was particularly relevant for mapping *P. radiata* (Fig. 3). This is because *P. radiata* have a conical crown shape that clearly differs from the native broadleaved species (Ishii and Asano 2010). Contrarily *A. dealbata* and *U. europaeus* have relatively similar crown shapes and structure as the native flora. The structural specifics of conifer species were found to be well captured in UAV-based 3D structural metrics also in other studies (Franklin et al. 2017).

Generally, the canopy-level information (1–4 m window size) outperformed the branch-level information (0.25–1 m window size) for both 2D texture and 3D structure variables. This indicates that branch characteristics—for example, branch form, branch orientation and leaf clumping—are less important than canopy differences. The importance of 2D textural metrics was found also in other studies (Michez et al., 2016; Lu & He, 2017; Cao et al., 2018). It can be assumed that, in contrast to information of single pixels (e.g. as for RGB or hyperspectral predictors), the textural metrics are less affected by small-scale variations, since these metrics are based on larger spatial scales (0.25–4 m). Moreover, it can be assumed that the texture metrics can even bundle this spatial variation (e.g. small-scale variation of sunlit and shaded crowns) in information that facilitates the classification task.

We found significant performance differences based on the validations in sunlit and shaded canopies in almost all cases (Table 2). This also applied for models trained with only structural information, indicating that shadows also hampered the creation of the photogrammetric point

clouds (performed in Agisoft Photoscan, Agisoft, Russia). Nevertheless, for spectral variables (especially RGB) the predicted rel. likelihood differed stronger between models including and excluding shadows from the calibration than for 2D textural and 3D structural variables (Fig. 4). This was more pronounced in *P. radiata* than for the other two species. We assume that spectral predictors were more affected by shadows in *P. radiata*, because of its more complex canopy structure and higher shadow fraction (Fig. 6c).

For all species we observed false negatives, that were spread in a rather scattered manner (Fig. 4). One option to address this issue could be to apply pre- and post-processing techniques, such as local filters (e.g. clump and sieve operators) and object-based analysis. Object-based analysis is known to decrease the so called salt-and-pepper effect caused by pixel-based classifications (Yu et al. 2006). This is one, reason why many previous UAV-based invasive species mapping studies used it. These studies did not considered the elimination of shadows prior to the allocation of spectral values to the segmented clumps (e.g. Alvarez-Taboada et al. 2017; Baena et al. 2017; Cao et al. 2018). Integrating both sunlit and shaded canopy reflectance into the segments could hamper the success of classification tasks if shadows are considered as noise.

Classification approach

One-class classifiers (OCC) are promising for invasive species mapping as only presence data of the target species are needed, decreasing field and laboratory work (hence being appealing for management agencies). MaxEnt is considered to be a robust and transferable OCC (Duque-Lazo et al. 2016) that yield high performances compared to other OCC algorithms in remote sensing applications (Stenzel et al. 2017). Because MaxEnt is very CPU demanding (Mack et al. 2016), especially combined with bootstrapping validation, we reduced CPU processing time using a comparable small set of presence/background samples. We used 500/2,000 instead of the sometimes recommended ~5000/10 000 presences/background samples (e.g. Stenzel et al. 2017). We compared MaxEnt performances for the *structtexthyper* independent variables (median accuracies and predictions) using 500/2000 and 5000/10 000 presence/background samples with a 10-fold cross validation for the three species and found no marked differences. Hence, we assume that the lower number of samples did not affect our result notably in this study.

Conclusions

Here, we investigated the effects of shadows on the predicted occurrences of three woody invasive species of central-south Chile using spectral (RGB and hyperspectral data), 2D textural and 3D structural variables derived from photogrammetry.

We found that shadows significantly affect the results of models trained with all types of variables. Areas with shadows obtained misclassification rates between 65% and 100%, even when shadows were included during model calibration. Particularly spectral and 2D textural variables were affected by shadows, leading to inaccurate model predictions in shaded areas and resulting in an increase of false negative predictions. Accordingly, the use of UAVs for mapping invasive plant species benefits from *ad hoc* pre-processing. The exclusion of shadows prior to model calibrations improved model predictions in all cases, especially in terms of false positives. Most accurate and robust results were usually obtained when combining spectral, 2D textural and 3D structural information. The use of hyperspectral instead of RGB data improved accuracies only for one of the three species (i.e. *U. europaeus*). Finally, the performed shadow simulations based on the photogrammetric digital surface models demonstrated that each species-specific canopy structure result in different shadow fractions during the course of a day. *P. radiata* showed a comparably narrow time period with a small shadow fraction. The rather smooth canopies of *A. dealbata* and *U. europaeus* resulted in a longer time span during the day with smaller shadow fractions. Hence, UAV data acquisitions need careful planning to minimize shadows and their related problems in species mapping applications. From the results of this investigation we hypothesize that shadows should not be used during calibration when pixel-based classifiers are used. Nevertheless, we do not discard the possibility that the negative effects of shadows on classification results could be reduced using approaches that include complex neighborhood information as information (e.g. deep learning). More investigation is needed to decrease the large amount of false negatives produced by shadows.

Acknowledgments

their work digitalizing training areas, Julian Cabezas, Jaime Hernandez, Tobias Schmidt and Birgit Kleinschmidt for helping in the UAV campaigns, and Rocio A. Araya-López and Michael Ewald for their useful comments on the paper.

Data Accessibility

R and Python codes used in the analysis can be accessed at: https://github.com/JavierLopatin/UAV-InvasiveSpp.

References

Adeline, K. R. M., M. Chen, X. Briottet, S. K. Pang, and N. Paparoditis. 2013. Shadow detection in very high spatial resolution aerial images: a comparative study. *ISPRS J. Photogramm. Remote Sens.* **80**, 21–38. https://doi.org/10.1016/j.isprsjprs.2013.02.003.

Alvarez-Taboada, F., C. Paredes, and J. Julián-Pelaz. 2017. Mapping of the invasive species Hakea sericea using Unmanned Aerial Vehicle (UAV) and worldview-2 imagery and an object-oriented approach. *Remote Sens.* **9**, (913). 17. https://doi.org/10.3390/rs9090913

Anderson, K., and K. J. Gaston. 2013. Lightweight unmanned aerial vehicles will revolutionize spatial ecology. *Front. Ecol. Environ.* **11**, 138–146. https://doi.org/10.1890/120150.

Araya-López, R. A., J. Lopatin, F. E. Fassnacht, and H. J. Hernández. 2018. Monitoring Andean high altitude wetlands in central Chile with seasonal optical data: a comparison between Worldview-2 and Sentinel-2 imagery. *ISPRS J. Photogramm. Remote Sens.* **145**. https://doi.org/10.1016/j.isprsjprs.2018.04.001

Baena, S., J. Moat, O. Whaley, and D. S. Boyd. 2017. Identifying species from the air: UAVs and the very high resolution challenge for plant conservation. *PLoS ONE* **12**, 1–21. https://doi.org/10.1371/journal.pone.0188714.

Binggeli, P. 1996. A taxonomic, biogeographical and ecological overview of invasive woody plants. *J. Veg. Sci.* **7**, 121–124.

Brodu, N., and D. Lague. 2012. 3D terrestrial lidar data classification of complex natural scenes using a multi-scale dimensionality criterion: applications in geomorphology. *ISPRS J. Photogramm. Remote Sens.* **68**, 121–134. https://doi.org/10.1016/j.isprsjprs.2012.01.006.

Cacho, J. O., D. Spring, P. Pheloung, and S. Hester. 2006. Evaluating the feasibility of eradicating an invasion. *Biol. Invasions* **8**, 903–917. https://doi.org/10.1007/s10530-005-4733-9.

Cao, J., W. Leng, K. Liu, L. Liu, Z. He, and Y. Zhu. 2018. Object-Based mangrove species classification using unmanned aerial vehicle hyperspectral images and digital surface models. *Remote Sens.* **10**(89). 20. https://doi.org/10.3390/rs10010089

Castillo-Riffart, I., M. Galleguillos, J. Lopatin, and J. F. Perez-Quezada. 2017. Predicting vascular plant diversity in anthropogenic peatlands: comparison of modeling methods with free satellite data. *Remote Sens.* **9**, 681. https://doi.org/10.3390/rs9070681.

Clapp, R. A. 1995. The unnatural history of the Monterey pine. *Geogr. Rev.* **85**, 1–19.

Duque-Lazo, J., H. van Gils, T. A. Groen, and R. M. Navarro-Cerrillo. 2016. Transferability of species distribution models: the case of Phytophthora cinnamomi in Southwest Spain and Southwest Australia. *Ecol. Model.* **320**, 62–70. https://doi.org/10.1016/j.ecolmodel.2015.09.019.

Dyrmann, M., H. Karstoft, and H. S. Midtiby. 2016. Plant species classification using deep convolutional neural network. *Biosys. Eng.* **151**, 72–80. https://doi.org/10.1016/j.biosystemseng.2016.08.024.

Franklin, S. E., O. S. Ahmed, and G. Williams. 2017. Northern conifer forest species classification using multispectral data acquired from an unmanned aerial vehicle. *Photogramm. Eng. Remote Sensing* **83**, 501–507. https://doi.org/10.14358/PERS.83.7.501.

Fuentes-Ramírez, A., A. Pauchard, L. A. Cavieres, and R. A. García. 2011. Survival and growth of *Acacia dealbata* vs. native trees across an invasion front in south-central Chile. *For. Ecol. Manage.* **261**, 1003–1009. https://doi.org/10.1016/j.foreco.2010.12.018

Gu, L., and A. Robles-Kelly. 2014. Shadow modelling based upon Rayleigh scattering and Mie theory. *Pattern Recogn. Lett.* **43**, 89–97. https://doi.org/10.1016/j.patrec.2013.10.020.

Holmgren, M., R. Avilés, L. Sierralta, A. M. Segura, and E. R. Fuentes. 2000. Why have European herbs so successfully invaded the Chilean matorral? Effects of herbivory, soil nutrients, and fire. *J. Arid Environ.* **44**, 197–211.

Hruska, R., J. Mitchell, M. Anderson, and N. F. Glenn. 2012. Radiometric and geometric analysis of hyperspectral imagery. *Remote Sens.* **4**, 2736–2752. https://doi.org/10.3390/rs4092736.

Huang, C., and G. P. Asner. 2009. Applications of Remote Sensing to Alien Invasive Plant Studies. *Sensors* **9**, 4869–4889. https://doi.org/10.3390/s90604869.

Ishida, T., J. Kurihara, F. A. Viray, S. B. Namuco, E. C. Paringit, G. J. Perez, et al. 2018. A novel approach for vegetation classification using UAV-based hyperspectral imaging. *Comput. Electron. Agr.* **144**, 80–85. https://doi.org/10.1016/j.compag.2017.11.027.

Ishii, H., and S. Asano. 2010. The role of crown architecture, leaf phenology and photosynthetic activity in promoting complementary use of light among coexisting species in temperate forests. *Ecol. Res.* **25**, 715–722. https://doi.org/10.1007/s11284-009-0668-4.

Jueterbock, A., I. Smolina, J. A. Coyer, and G. Hoarau. 2016. The fate of the Arctic seaweed Fucus distichus under climate change: an ecological niche modeling approach. *Ecol. Evol.* **6**, 1712–1724.

Kaplan, H., A. van Niekerk, J. J. Le Roux, D. M. Richardson, and J. R. U. Wilson. 2014. Incorporating risk mapping at multiple spatial scales into eradication management plans.

Biol. Invasions **16**, 691–703. https://doi.org/10.1007/s10530-013-0611-z.

Kattenborn, T., M. Sperlich, K. Bataua, and B. Koch. 2014. Automatic single palm tree detection in plantations using UAV-based photogrammetric point clouds. Pp. 139–144 *in* ISPRS ed.*International archives of the photogrammetry, remote sensing and spatial information sciences - ISPRS archives* (Vol. **40**). Remote Sensing and Spatial Information Sciences, Zurich, Switzerland. https://doi.org/10.5194/isprsarchives-xl-3-139-2014

Kattenborn, T., J. Lopatin, G. Kattenborn, and F. E. Fassnacht. 2018a. Pilot study on the retrieval of DBH and diameter distribution of deciduous forest stands using cast shadows in UAV-based ortomosaics. *ISPRS Ann. Photogramm. Remote Sens. Spatial Inform. Sci.* **IV-1**, 10–12. https://doi.org/10.5194/isprs-annals-iv-1-93-2018

Kattenborn, T., F. E. Fassnacht, and S. Schmidtlein. 2018b. Differentiating plant functional types using reflectance: which traits make the difference? *Remote Sens. Ecol. Conserv.* 1–15. https://doi.org/10.1002/rse2.86

Kohavi, R. 1995. A study of cross-validation and bootstrap for accuracy estimation and model selection. *Proc. Int. Joint Conf. Artificial Intelligence* **2**, 1137–1143.

Little, C., J. G. Cuevas, A. Lara, M. Pino, and S. Schoenholtz. 2015. Buffer effects of streamside native forests on water provision in watersheds dominated by exotic forest plantations. *Ecohydrology* **8**, 1205–1217. https://doi.org/10.1002/eco.1575.

Liu, W., and F. Yamazaki. 2012. Object-based shadow extraction and correction of high-resolution optical satellite images. *IEEE J. Select. Topics Appl. Earth Obs. Remote Sens.* **5**, 1296–1302. https://doi.org/10.1109/JSTARS.2012.2189558.

Lopatin, J., K. Dolos, H. J. Hernández, M. Galleguillos, and F. E. Fassnacht. 2016. Comparing Generalized Linear Models and random forest to model vascular plant species richness using LiDAR data in a natural forest in central Chile. *Remote Sens. Environ.* **173**, 200–210. https://doi.org/10.1016/j.rse.2015.11.029.

Lopatin, J., F. E. Fassnacht, T. Kattenborn, and S. Schmidtlein. 2017. Mapping plant species in mixed grassland communities using close range imaging spectroscopy. *Remote Sens. Environ.* **201**, 12–23. https://doi.org/10.1016/j.rse.2017.08.031.

Luebert, F., and P. Pliscoff. 2006. *Sinopsis bioclimática y vegetacional de Chile Santiago de Chile*. Editorial Universitaria, Santiago, Chile. 316 p.

Mack, B., R. Roscher, S. Stenzel, H. Feilhauer, S. Schmidtlein, and B. Waske. 2016. Mapping raised bogs with an iterative one-class classification approach. *ISPRS J. Photogramm. Remote Sens.* **120**, 53–64. https://doi.org/10.1016/j.isprsjprs.2016.07.008.

Mafanya, M., P. Tsele, J. Botai, P. Manyama, B. Swart, and T. Monate. 2017. Evaluating pixel and object based image classification techniques for mapping plant invasions from UAV derived aerial imagery: *Harrisia pomanensis* as a case study. *ISPRS J. Photogramm. Remote Sens.* **129**, 1–11. https://doi.org/10.1016/j.isprsjprs.2017.04.009.

Merow, C., M. J. Smith, and J. A. Silander. 2013. A practical guide to MaxEnt for modeling species' distributions: what it does, and why inputs and settings matter. *Ecography* **36**, 1058–1069. https://doi.org/10.1111/j.1600-0587.2013.07872.x.

Michez, A., H. Piégay, L. Jonathan, H. Claessens, and P. Lejeune. 2016. Mapping of riparian invasive species with supervised classification of Unmanned Aerial System (UAS) imagery. *Int. J. Appl. Earth Obs. Geoinf.* **44**, 88–94. https://doi.org/10.1016/j.jag.2015.06.014.

Milas, A. S., K. Arend, C. Mayer, M. A. Simonson, and S. Mackey. 2017. Different colours of shadows: classification of UAV images. *Int. J. Remote Sens.* **38**, 3084–3100. https://doi.org/10.1080/01431161.2016.1274449.

Müllerová, J., J. Brůna, T. Bartaloš, P. Dvořák, M. Vítková, and P. Pyšek. 2017. Timing is important: unmanned aircraft vs. satellite imagery in plant invasion monitoring. *Front. Plant Sci.* **8**, 1–13. https://doi.org/10.3389/fpls.2017.00887

Myers, N., R. A. Mittermeier, C. G. Mittermeier, G. A. B. da Fonseca, and J. Kent. 2000. Biodiversity hotspots for conservation priorities. *Nature* **403**, 853–858. https://doi.org/10.1038/35002501.

Nagendra, H. 2001. Using remote sensing to assess biodiversity. *Int. J. Remote Sens.* **22**, 2377–2400. https://doi.org/10.1080/01431160117096.

Nevalainen, O., E. Honkavaara, S. Tuominen, N. Viljanen, T. Hakala, X. Yu, et al. 2017. Individual tree detection and classification with UAV-based photogrammetric point clouds and hyperspectral imaging. *Remote Sens.* **9**, 185. https://doi.org/10.3390/rs9030185

Norambuena, H., S. Escobar, and F. Rodriguez. 2000. The Biocontrol of Gorse, *Ulex europaeus*, in Chile: a Progress Report. Pp. 955–961 *in* N. R. Spencer, ed. *Proceedings of the International symposium on biological control of weeds*. Montana State University, Bozeman, Montana, USA.

Phillips, S. J., R. P. Anderson, and R. E. Schapire. 2006. Maximum entropy modeling of species geographic distributions. *Ecol. Model.* **190**, 231–259. https://doi.org/10.1016/j.ecolmodel.2005.03.026.

Ricciardi, A., M. E. Palmer, and N. D. Yan. 2011. Should biological invasions be managed as natural disasters? *Bioscience* **61**, 312–317. https://doi.org/10.1525/bio.2011.61.4.11.

Richardson, D. M., C. Hui, M. A. Nuñez, and A. Pauchard. 2014. Tree invasions: patterns, processes, challenges and opportunities. *Biol. Invasions* **16**, 473–481. https://doi.org/10.1007/s10530-013-0606-9.

Rocchini, D., V. Andreo, M. Förster, C. X. Garzon-Lopez, A. P. Gutierrez, T. W. Gillespie, et al. 2015. Potential of remote sensing to predict species invasions: a modelling perspective. *Prog. Phys. Geogr.* **39**, 283–309. https://doi.org/10.1177/0309133315574659.

de Sá, N. C., P. Castro, S. Carvalho, E. Marchante, F. A. López-Núñez, and H. Marchante. 2018. Mapping the flowering of an invasive plant using unmanned aerial vehicles: is there potential for biocontrol monitoring? *Front Plant Sci.* **9**, 1–13. https://doi.org/10.3389/fpls.2018.00293

Saha, A. K., M. K. Arora, E. Csaplovics, and R. P. Gupta. 2005. Land cover classification using IRS LISS III image and DEM in a rugged terrain: a case study in Himalayas. *Geocarto Int.* **20**, 33–40. https://doi.org/10.1080/10106040508542343.

Singh, K. K., K. Pal, and M. J. Nigam. 2012. Shadow detection and removal from remote sensing images using NDI and morphological operators. *Int. J. Comp. Appl.* **42**, 37–40. https://doi.org/10.5120/5731-7805.

Sismanidis, P., V. Karathanassi, and P. Kolokoussis. 2014. De-shadowing of airborne imagery using at-sensor downwelling irradiance data. *Int. J. Remote Sens.* **35**, 6973–6992. https://doi.org/10.1080/01431161.2014.960620.

Skowronek, S., M. Ewald, M. Isermann, R. Van De Kerchove, J. Lenoir, R. Aerts, et al. 2017. Mapping an invasive bryophyte species using hyperspectral remote sensing data. *Biol. Invasions* **19**, 239–254. https://doi.org/10.1007/s10530-016-1276-1.

Stenzel, S., F. E. Fassnacht, B. Mack, and S. Schmidtlein. 2017. Identification of high nature value grassland with remote sensing and minimal field data. *Ecol. Ind.* **74**, 28–38. https://doi.org/10.1016/j.ecolind.2016.11.005.

Vilà, M., J. L. Espinar, M. Hejda, P. E. Hulme, V. Jarošík, J. L. Maron, et al. 2011. Ecological impacts of invasive alien plants: a meta-analysis of their effects on species, communities and ecosystems. *Ecol. Lett.* **14**, 702–708. https://doi.org/10.1111/j.1461-0248.2011.01628.x.

Weinacker, H., B. Koch, and R. Weinacker. 2004. TREESVIS—a software system for simultaneous 3D-realtime visualization of DTM, DSM, laser raw data, multispectral data, simple tree and building models. *Int. Arch. Photogrametry Remote Sens. Spat. Inf. Sci.* **XXXVI**, 90–95.

Westoby, M. J., J. Brasington, N. F. Glasser, M. J. Hambrey, and J. M. Reynolds. 2012. 'Structure-from-Motion' photogrammetry: a low-cost, effective tool for geoscience applications. *Geomorphology* **179**, 300–314. https://doi.org/10.1016/j.geomorph.2012.08.021.

Yu, Q., P. Gong, N. Clinton, G. Biging, M. Kelly, and D. Schirokauer. 2006. Object-based detailed vegetation classification with airborne high spatial resolution remote sensing imagery. *Photogramm. Eng. Remote Sensing* **72**, 799–811. https://doi.org/10.14358/PERS.72.7.799.

Zhang, L., X. Sun, T. Wu, and H. Zhang. 2015. An analysis of shadow effects on spectral vegetation indexes using a ground-based imaging spectrometer. *IEEE Geosci. Remote Sens. Lett.* **12**, 2188–2192. https://doi.org/10.1109/LGRS.2015.2450218.

Supporting Information

Additional supporting information may be found online in the Supporting Information section at the end of the article.

Table S1. Parameterization of Agisoft Photoscan. Settings not included were set as default.

Figure S1. Model performances for sunlit (A) and shaded (B) canopies using models that include (incl.) and exclude (excl.) shadows in the calibration data. The coefficient of variation (CV) iterative values are presented, with dot size scaled to the values. *A.d.* = *Acacia dealbata*; *U.e.* = *Ulex europaeus*; *P.r.* = *Pinus radiata*. * depicts significant ($\alpha = 0.05$) improvements of the models excluding shaded canopies over the models including shaded canopies (A) and of the models including shaded canopies over the models excluding shaded canopies (B).

Figure S2. Significant differences in terms of model performance among models using models excluding shadows in the calibration data.